Physics of the Solid State, 2025, Vol. 67, No. 9

13,07

The crystal structure features of Ca-substituted ferrites $La_{1-x}Ca_xFeO_{3-y}$

© V.D. Sedykh[1], V.S. Rusakov[2], O.G. Rybchenko[1], A.M. Gapochka[2], M.E. Mutsnev[2], A.A. Toporkova[1], A.I. Ivanov[1], V.I. Kulakov[1]

[1] Osipyan Institute of Solid State Physics RAS, Chernogolovka, Russia
[2] Moscow State University, Moscow, Russia

E-mail: sedykh@issp.ac.ru

Received May 25, 2025
Revised August 28, 2025
Accepted August 29, 2025

The crystal structure features of the Ca-substituted lanthanum ferrite $La_{1-x}Ca_xFeO_{3-y}$ have been studied as the Ca concentration dependence ($x = 0.0$, 0.3, 0.5, 0.7, 1.0) using X-ray diffraction analysis and Mössbauer spectroscopy. It has been investigated both the synthesized samples and the samples annealed at 650 °C in vacuum, when Fe^{4+} ions are completely transferred to Fe^{3+}. When the Ca concentration is $x < 0.5$, the *Pbnm* orthorhombic phase is formed. At higher Ca concentrations ($x > 0.5$) — the vacancy-ordered Grenier ($LaCa_2Fe_3O_8$) and Brounmillerite ($Ca_2Fe_2O_5$) phases are formed. The portion of each valence Fe state, the number of oxygen vacancies, and oxygen content were determined using the low-temperature Mössbauer data for all the samples studied. The synthesized sample with $x = 0.5$ has a maximum number of Fe^{4+} ions. The Fe ions are in a trivalent state for the initial and last numbers of the concentration series, $x = 0$ ($LaFeO_3$) and $x = 1$ ($Ca_2Fe_2O_5$). In the synthesized samples, the relation of contributions of the different Fe^{3+} ion structural states to the Mössbauer spectrum has been shown to change towards the oxygen environments characteristic of the vacancy-ordered phases when increasing Ca concentration. The vacuum annealing (when there are no Fe^{4+} ions) results in the formation of lower defective local environment of Fe ions.

Keywords: orthoferrites, Fe valence states, oxygen vacancies, Mössbauer spectroscopy, X-ray diffraction.

DOI: 10.61011/PSS.2025.09.62365.139-25

1. Introduction

Due to their unusual electrical, magnetic and catalytic properties, perovskite-like compounds with heterovalent substitution of the type $R_{1-x}A_xBO_{3-y}$, where R is a rare earth element, A is an alkaline earth element (Ba, Ca or Sr), B is a transition metal (Fe, Mn, Co or Ni), are promising materials in the wide field of their application: as fuel-cell electrodes, catalysts, gas sensors, optoelectronic devices and magnetic memory devices [1–6]. Due to presence of oxygen vacancies, these compounds also have antibacterial properties [7].

In the systems $R_{1-x}A_xBO_{3-y}$, ions of the transition metals (B) have mixed valence states, thereby providing high electron conductivity at the room temperature [8]. The mixed valence state is formed to compensate charge disbalance, it can appear both when substituting a trivalent element (R) with a bivalent one (A) and when there are oxygen vacancies. Oxygen nonstoichiometry induces high ion conductivity in terms of oxygen.

Antiferromagnetism in lanthanum ferrite $LaFeO_3$ is a result of superexchange interaction between cations Fe^{3+} and Fe^{3+} [9], which is stronger that interaction between ions Fe^{3+} and Fe^{4+} as well as Fe^{4+} and Fe^{4+} [10]. Therefore, presence of Fe^{4+} in substituted orthoferrites results in attenuation of antiferromagnetic interaction and, respectively, in reduction of the Néel temperature [11]. Thus, most special properties of the orthoferrites are related to presence of tetravalent iron and oxygen vacancies, whose content and distribution homogeneity in turn depend on a number of factors: a type and a portion of a lanthanum-substituting element, conditions of synthesis and subsequent thermal treatments. Using vacuum annealing as a tool of varying the vacancy content makes it possible to control a ratio of the valence states $Fe^{3+}:Fe^{4+}$ up to a complete transition into Fe^{3+}, when the lattice keeps only oxygen, whose amount is exclusively determined by a portion of the substituting element [12].

An important role in formation of a particular crystal lattice of the substituted lanthanum orthoferrite can be played by a difference in ionic radii of La and the substituting element. La substitution results in a change of a volume of the lattice cell in perovskite-type phases and can induce noticeable distortions of the crystal lattice as well as result in formation of layered ordered phases. All these factors also affect properties of the ferrites.

Two extreme compositions of the studied system — $LaFeO_3$ and $CaFeO_{2.5}$ — contain iron ions only in the trivalent state; wherein in $LaFeO_3$ they all are in an octahedral oxygen environment (the coordination number $K = 6$), whereas there are two oxygen environments in $CaFeO_{2.5}$: an octahedral one ($K = 6$) and a tetrahedral one ($K = 4$). A structure of the unsubstituted orthoferrites is quite well studied: $LaFeO_3$ [13,14] and the Brownmillerite phase $CaFeO_{2.5}$ with ordered arrangement of the oxygen vacancies [15,16], so is the structure of the Ca-substituted Grenier phase $LaCa_2Fe_3O_8$ [17,18]. The substituted orthoferrites $La_{1-x}Ca_xFeO_{3-\gamma}$ are studied in a lesser degree (for example, [19]). It especially concerns systematic studies — investigating the influence of the portion of the substituting element as well as its related quantitative ratio of the valence states $Fe^{3+}:Fe^{4+}$ and oxygen content on the structure and the physical properties.

Our previous studies [12,20–22] have investigated specific features of the structure (including at a local level) as well as magnetic properties of orthoferrites of the system $La_{1-x}Sr_xFeO_{3-\gamma}$, in which the ionic radius of the substituting element is higher than for lanthanum (1.44 Å for Sr^{2+}, 1.36 Å for La^{3+} [23]). The present study has used Ca^{2+} with the ionic radius (1.34 Å) that is less than that of La, as a substituting element and investigated a dependence of the crystal structure $La_{1-x}Ca_xFeO_{3-\gamma}$, the oxygen content as well as the valence states and the local environment of the Fe ions on the Ca portion x; and their changes after vacuum annealing have been studied.

2. Experiment

Polycrystalline samples of complex oxides $La_{1-x}Ca_xFeO_{3-\gamma}$ were produced by a glycine-nitrate method using $La(NO_3)_3 \cdot 6H_2O$ (of chemical purity, CP), $Ca(NO_3)_2 \cdot 4H_2O$ (CP), $Fe(NO_3)_3 \cdot 9H_2O$ (Acros Organics, $99+\%$) and glycine ($> 99.5\%$) as as-prepared components. Metal nitrates and glycine were dissolved in a required quantity in distilled water with intense stirring in a magnetic mixer. Evaporation and smoldering of a reaction mixture were followed by formation of a loose mass that was annealed in air at 900 °C for 2 h to remove carbon-containing residues. After that, it was finally annealed in air at 1200 °C with isothermal holding for 25 h. After synthesis, the samples were annealed in vacuum of 10^{-3} Torr at the temperature of 650 °C.

The polycrystalline samples were structurally qualified at the room temperature using the diffractometer Rigaku SmartLab SE with CuKα-radiation. Powder Cell 2.4 and Match3 software programs were used for phase analysis and determination of structural parameters.

The Mössbauer measurements of the polycrystalline samples were carried out at 85 K using a spectrometer SM 1101 designed to operate in a constant acceleration mode. A radioactive source $^{57}Co(Rh)$ was used for the experiment. The spectra were processed and analyzed by a method of model fitting using the SpectrRelax software [24].

3. Results and discussion

3.1. X-ray diffraction analysis

The as-prepared samples $LaFeO_3$ and $La_{0.7}Ca_{0.3}FeO_{3-\gamma}$ have an orthorhombic structure (the space group *Pbnm*). Partial replacement of lanthanum with Ca results in the change of the lattice cell parameters and, as a result, reduction (approximately by 2 %) of a crystal cell volume per one formula unit — the so-called perovskite cell volume (V_{cell}). It is related to the difference in the ionic radii of Ca^{2+} and La^{3+} (1.34 and 1.36 Å [23]) as well as changing the valence state of some Fe ions from Fe^{3+} to Fe^{4+}, which also have different ionic radii (Fe^{3+} — 0.645 Å, Fe^{4+} — 0.585 Å).

Vacuum annealing does not change the structure of $LaFeO_3$; the substituted lanthanum ferrite $La_{0.7}Ca_{0.3}FeO_{3-\gamma}$ is also still orthorhombic, but the perovskite cell volume V_{cell} increases from 59.08 to 59.77 Å^3.

With an increase of the Ca portion, lines on diffraction patterns of the as-prepared samples are noticeably widened. As shown by our previous studies [25], the ferrite samples synthesized by a sol-gel method have a small grain size (about several tens of nanometers), thereby resulting in broadening of the diffraction lines. At the same time, as follows from the literature [26], the average grain size decreases with an increase of the calcium concentration in $La_{1-x}Ca_xFeO_{3-\gamma}$. Another possible cause of the change of the width of the lines is lattice microdistortions that increase together with the concentration of the substituting Ca [27]. They seem to be related to the difference in the atomic radii of Ca^{2+} and La^{3+} as well as nonuniform distribution of originating oxygen vacancies, which correlates with distribution of the ions Ca^{2+} and La^{3+} according to necessity of local charge compensation. These distortions result in generation of a micro-unit structure.

The main phase in the as-prepared sample $La_{0.5}Ca_{0.5}FeO_{3-\gamma}$ also has an orthorhombic structure (the space group *Pbnm*), V_{cell} differs from the value for the unsubstituted lanthanum ferrite $LaFeO_3$ approximately by 4 %. The second phase is assumed to be a Grenier orthorhombic phase of the composition $Ca_2LaFe_3O_8$ (the space group $P2_1ma$, PDF-2 #01-082-3103) [17]. Its portion is small and some lines of its spectrum are superimposed on the lines *Pbnm*, while the others have a very low intensity, thereby complicating its identification.

The sample $La_{0.5}Ca_{0.5}FeO_{3-\gamma}$ after vacuum annealing also has two phases in its composition: the main one of them is with a cubic lattice ($Pm\overline{3}m$), while the impurity one in the amount of at most 10 % is the Grenier phase. In the diffraction pattern, lines of this phase, except for one, have a low intensity, but the obtained data and comparison with results for the as-prepared sample allow us to identify this phase as the Grenier phase quite confidently. Transformation of the orthorhombic phase into the cubic one is accompanied by the increase of the crystal lattice volume per one formula unit V_{cell} from 58.12 to 59.24 Å^3. Figure 1 shows diffraction patterns of the sample

$La_{0.5}Ca_{0.5}FeO_{3-\gamma}$ before and after vacuum annealing; the insert includes an angular interval that has the most intense lines of the Grenier phase and shows low-intensity lines $Pbnm$ that are absent in the spectrum of the phase with the cubic lattice $Pm\overline{3}m$.

The sample $La_{0.3}Ca_{0.7}FeO_{3-\gamma}$, both the as-prepared and vacuum-annealed one, consists of two phases, and a prevalent one of them is the Grenier phase (Figure 2). Its content in the as-prepared sample — $\sim 60\,\%$ insignificantly increases in the annealed one. The second phase in the as-prepared sample is an orthorhombic one $Pbnm$, whose structure is changed into the cubic one as a result of annealing in the same way as in $La_{0.5}Ca_{0.5}FeO_{3-\gamma}$.

The nature of the cubic phase observed by us in the annealed samples $La_{0.5}Ca_{0.5}FeO_{3-\gamma}$ and $La_{0.3}Ca_{0.7}FeO_{3-\gamma}$ has been discussed in some studies carried out using high-resolution electron microscopy and electron diffraction [28–31]. As shown by these experiments, the Ca-substituted lanthanum ferrites are characterized by formation of a microdomain structure that consists of disoriented domains with sizes of about tens of nanometers and is pictured as a perovskite cube in X-ray diffraction. A type of the domain structure depends on the ratio Ca : La and domains with a different structure can merge, for example, the Grenier phase and the Brownmillerite. The transformation from $Pbnm$ into the perovskite cube, which is observed by us during vacuum annealing, is probably related to formation of the microdomains with the Grenier-phase structure. In case of the composition $La_{0.5}Ca_{0.5}FeO_{3-\gamma}$ these micro units possibly coexist with the domains with the structure $Pbnm$ (the local structure is determined by distribution of Ca and La), while in the sample $La_{0.3}Ca_{0.7}FeO_{3-\gamma}$ they can almost completely have the Grenier phase.

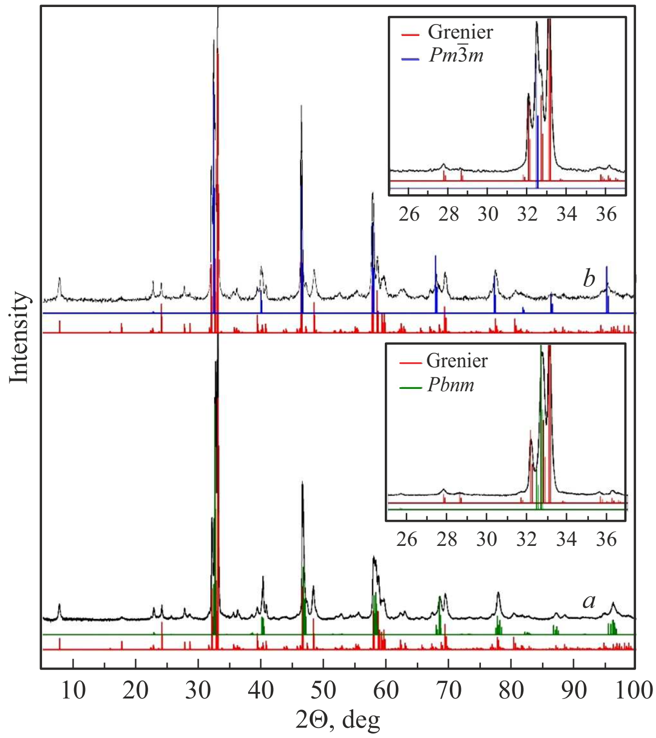

Figure 2. Diffraction patterns of the sample $La_{0.3}Ca_{0.7}FeO_{3-\gamma}$ a) before and after b) vacuum annealing. The inserts include respective fragments of the diffraction spectra in a limited angular range.

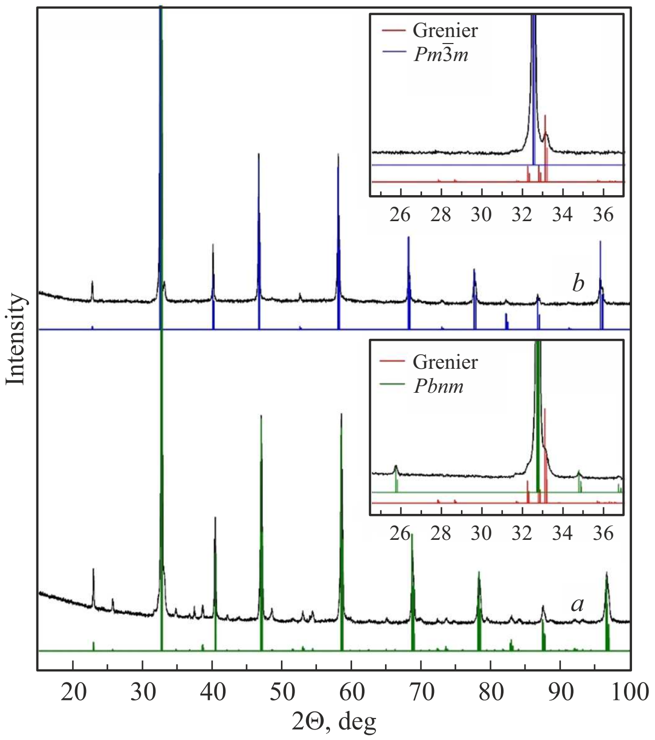

Figure 1. Diffraction patterns of the sample $La_{0.5}Ca_{0.5}FeO_{3-\gamma}$ a) before and b) after vacuum annealing. The inserts include respective fragments of the diffraction spectra in a limited angular range.

The sample that does not contain La has the Brownmillerite structure ($CaFeO_{2.5}$) both in the as-prepared and annealed state.

3.2. Mössbauer data

The Mössbauer spectra of the Ca-substituted orthoferrites $La_{1-x}Ca_xFeO_{3-\gamma}$ ($x = 0$, 0.3, 0.5, 0.7, 1) that are synthesized and annealed at 650 °C were measured at 85 K and are shown in Figure 3. The Mössbauer spectrum of the magnetic-ordered lanthanum orthoferrite $LaFeO_3$ ($x = 0$) is a typical Zeeman sextet with narrow lines (Figure 3). Values of hyperfine parameters of the spectrum: an isomer shift δ, a quadrupole shift ε and a hyperfine magnetic field H_{hf} (Table 1) well agree with known literature data [32] and correspond to trivalent iron atoms Fe^{3+} in the high-spin state, which are in the octahedral oxygen environment.

The Mössbauer spectrum of the magnetic-ordered calcium orthoferrite $CaFeO_{2.5}$ ($x = 1$) is a set of two sextets (Figure 3). The hyperfine parameters of the spectrum correspond to the trivalent iron atoms Fe^{3+} that are in the

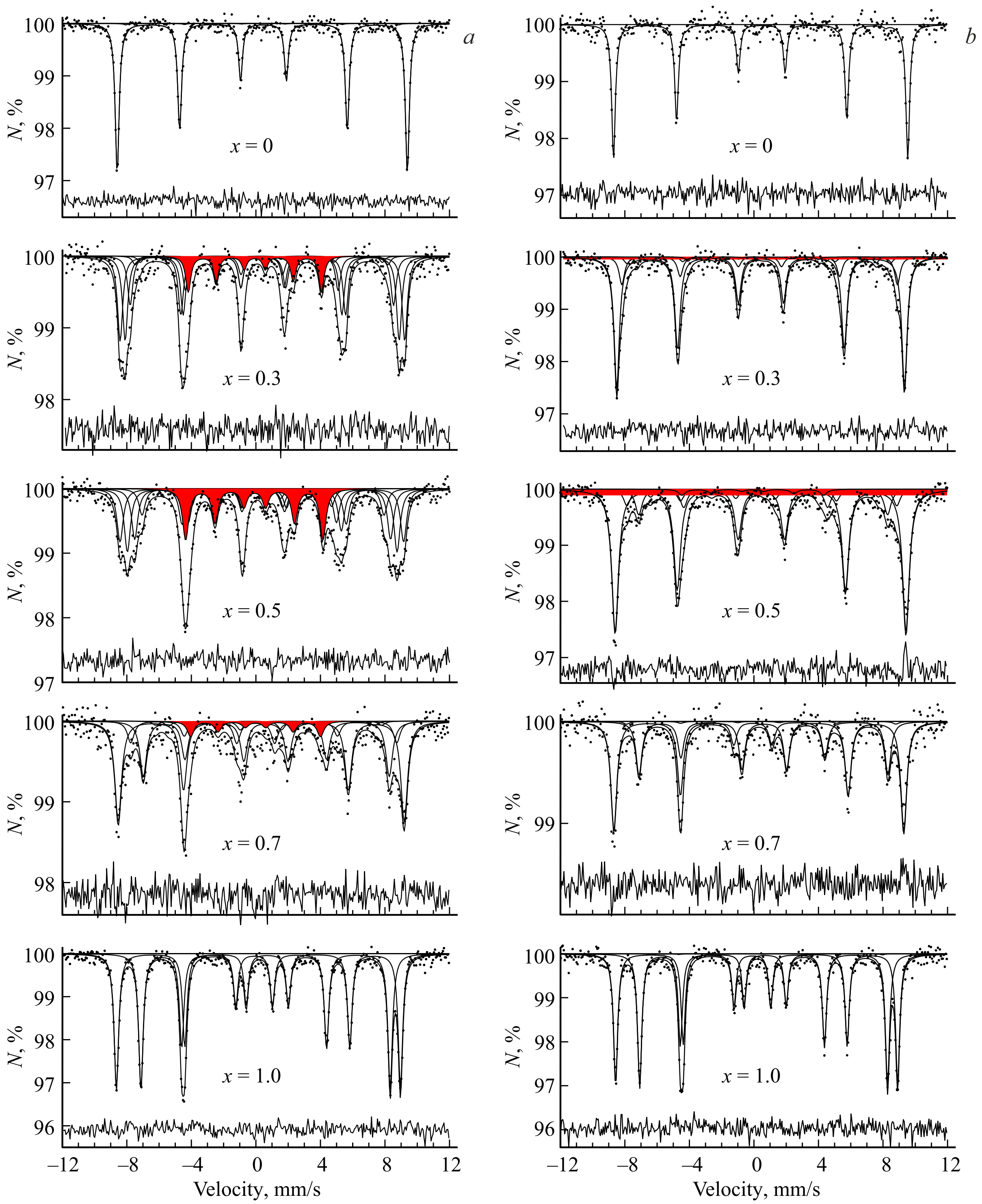

Figure 3. Results of model fitting of the Mössbauer spectra of the samples $La_{1-x}Ca_xFeO_{3-\gamma}$, which are measured at 85 K: *a*) the as-prepared ones *b*) and those annealed in vacuum at 650 °C. The subspectrum of the ions Fe^{4+} is highlighted in red. A difference spectrum is given below each experimental spectrum.

high-spin state in two oxygen environments: the octahedral one (with a higher hyperfine magnetic field and a higher isomer shift) and the tetrahedral one (Table 1).

A ratio of areas of two subspectra that correspond to these states of the iron atoms is 1 : 1. The spectrum corresponds to the Brownmillerite phase $Ca_2Fe_2O_5$ [15], which is well known in the literature and in which octahedral and tetrahedral layers are alternate.

Thus, a specific feature of the Ca-substituted orthoferrites is that in the two extreme synthesized samples with $x = 0$

Table 1. Results of model fitting of the Mössbauer spectra of lanthanum orthoferrite $LaFeO_3$ and calcium orthoferrite $CaFeO_{2.5}$

Sample	δ, mm/s	ε, mm/s	H_{hf}, kOe	I, %	Site of atom Fe
$LaFeO_3$	0.433(2)	−0.037(2)	556.4(6)	100	Octahedral
$CaFeO_{2.5}$	0.432(2)	−0.275(2)	540.1(5)	49.9(4)	Octahedral
	0.245(2)	0.354(2)	473.2(5)	50.1(4)	Tetrahedral

($LaFeO_3$) and $x = 1$ ($CaFeO_{2.5}$) the Fe ions are only in the trivalent state. But when $x = 0$ the sample has not oxygen vacancies and the Fe ions are in one oxygen environment, while when $x = 1$ the number of the vacancies is the highest and the Fe ions are in the two oxygen environments.

The spectra of the samples $La_{1-x}Ca_xFeO_{3-\gamma}$ ($x = 0.3$, 0.5, 0.7), which are measured at 85 K, consist of a set of several subspectra; the hyperfine parameters of one of them, which has the smaller shift and hyperfine field, correspond to the ions Fe^{4+}, while the others correspond to the ions Fe^{3+} (Figure 3). When substituting La^{3+} with Ca^{2+} in $LaFeO_3$ or Ca^{2+} with La^{3+} in $CaFeO_{2.5}$, the presence of several Zeeman sextets in the spectra, which belong to the ions Fe^{3+}, is related to appearance of the oxygen vacancies and the ions Fe^{4+} in the nearest ion environment of the ions Fe^{3+}, i.e. the Fe atoms with the mixed valence appear during substitution. Vacuum annealing of the as-prepared synthesized sample changes the number of the oxygen vacancies and the ions Fe^{4+}, thereby resulting in respective variation of the hyperfine parameters of the Mössbauer spectra. In accordance with the electroneutrality condition, a crystallochemical formula of the substituted ferrite $La_{1-x}Ca_xFeO_{3-\gamma}$ can be written as

$$La^{3+}_{1-x}Ca^{2+}_xFe^{3+}_{1-y}Fe^{4+}_yO^{2-}_{3-\gamma} \Rightarrow$$
$$\Rightarrow (La^{3+}_{1-x}Ca^{2+}_x)(Fe^{3+}_{1-x+2\gamma}Fe^{4+}_{x-2\gamma})(O^{2-}_{3-\gamma}\square_\gamma), \quad (1)$$

where x, $y = x - 2\gamma$ and $\gamma = (x - y)/2$ is an average number of the ions Ca^{2+}, Fe^{4+} and the oxygen vacancies ($\square$) per the formula unit of the ferrite, respectively. It is evident that hence follows an interrelation between the numbers x, y and γ.

With model fitting of the Mössbauer spectra, the number of the ions Ca^{2+} (x) is pre-defined, while the numbers of the ions Fe^{4+} (y) and the oxygen vacancies (γ) are calculated. If it is assumed that probabilities of the Mössbauer effect for the ^{57}Fe nuclei belonging to the ions Fe^{3+} and Fe^{4+} are almost the same, then relative areas of their subspectra make it possible to determine for each sample not only the number of the ions Fe^{4+} (y), but the number of the oxygen vacancies (γ) and anions O^{2-} ($3 - \gamma$) per the formula unit for pre-defined substitution of the ions La^{3+} with the ions Ca^{2+} (x):

$$y = \frac{I(Fe^{4+})}{I(Fe^{4+}) + I(Fe^{3+})}, \quad \gamma = (x - y)/2. \quad (2)$$

Here, $I(Fe^{4+})$ and $I(Fe^{3+})$ are relative areas of the Mössbauer subspectra of the ions Fe^{4+} and Fe^{3+}, respectively. At the same time, it is easy to calculate an average number n of the cations Fe^{4+}, the oxygen vacancies $\square$ and the oxygen ions O^{2-} in the nearest cation and anion environments of the Fe atom:

$$n(Fe^{4+}) = 6y, \quad n(\square) = 2\gamma = x - y,$$
$$n(O^{2-}) = 6 - 2\gamma = 6 - (x - y). \quad (3)$$

Taking into account possible values of the number of the oxygen vacancies (γ) and the number of the ions Fe^{4+} (y), the experimental spectra were fitted in an assumption that there are up to five subspectra of Fe^{3+} and one subspectrum of Fe^{4+} (see Figure 3). Appearance of the oxygen vacancy in the nearest environment of the ion Fe^{3+} breaks an exchange bond Fe^{3+}–O^{2-}–Fe, thereby resulting in reduction of the hyperfine magnetic field H_{hf} and a change of the isomer shift of the spectrum [33,34]. Appearance of the ion Fe^{4+} in the nearest cation environment of the ion Fe^{3+} results in weakening of the exchange bond and, respectively, reduction of the field H_{hf}. Let us introduce into consideration a number of broken and weakened bonds m and assume that changes of the hyperfine field, the isomer shift and the quadrupole shift for the subspectra of the ions Fe^{3+} in the samples are almost the same with an increase of the number m of either breaks or weakening of the exchange bonds, as induced by appearance of either the oxygen vacancies or the ions Fe^{4+}:

$$H_{hf}(Fe^{3+}; m) = H_{hf}(Fe^{3+}; 0) + m\Delta H_{hf}(Fe^{3+}), \quad (4)$$

$$\delta(Fe^{3+}; m) = \delta(Fe^{3+}; 0) + m\Delta\delta(Fe^{3+}), \quad (5)$$

$$\varepsilon(Fe^{3+}; m) = \varepsilon(Fe^{3+}; 0) + m\Delta\varepsilon(Fe^{3+}). \quad (6)$$

Here, $H_{hf}(Fe^{3+}; 0)$, $\varepsilon(Fe^{3+}; 0)$ and $\delta(Fe^{3+}; 0)$ are values of the hyperfine field, the isomer shift and the quadrupole shift for the subspectrum of the ions Fe^{3+} when $m = 0$, i.e. with all the six exchange bonds Fe^{3+}–O^{2-}–Fe^{3+} without the oxygen vacancies and the ions Fe^{4+} in the nearest environment; $\Delta H_{hf}(Fe^{3+})$, $\Delta\delta(Fe^{3+})$ and $\Delta\varepsilon(Fe^{3+})$ are changes of the hyperfine field, the isomer shift and the quadrupole shift during either breaking or weakening of one exchange bond. The above-described model was used to adequately describe the Mössbauer spectra of the substituted lanthanum ferrites $La_{1-x}Ca_xFeO_{3-\gamma}$ measured at the temperature of 85 K: as a result of model fitting of the spectra, values of the normalized functional χ^2 were

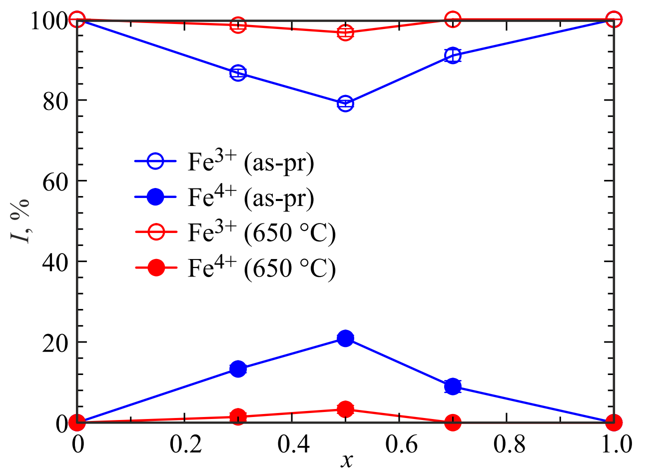

Figure 4. Dependences of relative areas I of the spectra of the ions Fe^{3+} and Fe^{4+} on the Ca content (x) in the as-prepared (as-pr) samples and in the samples annealed at 650 °C in vacuum.

within the interval 0.93−1.16, and at the same time, as it is clear in Figure 3, the difference spectra had not systematic deviations.

Figure 4 shows dependences of relative areas of the subspectra of all the ions Fe^{3+} and the ions Fe^{4+} for the as-prepared and vacuum-annealed samples on the Ca concentration, which are obtained as a result of model fitting of the experimental Mössbauer spectra.

As it is clear in the figure, with the increase of the Ca concentration in the as-prepared samples, the area of the subspectrum that corresponds to Fe^{4+} increases, while for $x \geq 0.5$ it decreases, reaching zero when $x = 1$ ($CaFeO_{2.5}$).

Using data obtained as a result of model fitting, for the synthesized samples annealed at 650 °C, one can obtain the dependences of relative areas $I(Fe^{3+}; m)$ of the subspectra of the ions Fe^{3+} on the number m of either broken or weakened exchange bonds, as induced by appearance of either the oxygen vacancies or the ions Fe^{4+} in the nearest environment of the ions Fe^{3+}, which are shown in Figure 5. At the same time, if one assumes random distribution of the oxygen vacancies and the ions Fe^{4+} along their crystallographic sites, then it is possible to calculate probabilities p of presence of the cation Fe^{4+}, the oxygen vacancy $\square$ and the oxygen ion O^{2-} in the nearest cation and anion environments of the Fe atom:

$$p(Fe^{4+}) = y, \quad p(\square) = \gamma/3 = (x-y)/6,$$
$$p(O^{2-}) = (3-\gamma)/3 = 1-(x-y)/6, \qquad (7)$$

as well as probability of appearance of either the oxygen vacancy or the ion Fe^{4+}, i.e. either break or weakening of the exchange bonds $p(\square \vee Fe^{4+})$:

$$p(\square \vee Fe^{4+}) = p(\square) + p(Fe^{4+}) - p(\square)p(Fe^{4+})$$
$$= x/6 + y5/6 - xy/6 + y^2/6. \qquad (8)$$

For comparison according to (8), Figure 5 also shows binomial distributions of the number m of breaks or weakening of the exchange bonds. As it is clear, the assumption on random distribution of the oxygen vacancies and the ions Fe^{4+} can be applied only when $x \leq 0.5$ for the as-prepared samples and when $x \leq 0.3$ for the annealed samples. With the increase of x, when ordered phases (with oxygen-vacancy ordering) start being formed, this assumption is no longer valid.

With the increase of the Ca concentration, contributions into the Mössbauer spectrum by various structure states of Fe^{3+} are redistributed.

After vacuum annealing, when the ions Fe^{4+} transfer to Fe^{3+}, the pattern is noticeably changed (Figure 5, b). It is especially manifested for the subspectra $I(Fe^{3+}; m = 0)$ and $I(Fe^{3+}; m = 2)$. As a result, with the increase of the Ca concentration, their ratio when $x = 1$ is 1:1, which corresponds to the Brownmillerite phase $Ca_2Fe_2O_5$ with a ratio of the layers with the octahedral and tetrahedral oxygen environment of the ions Fe^{3+} being 1:1. When $x = 0.7$, in the annealed samples the ratio of areas of the subspectra $I(Fe^{3+}; m = 0)/I(Fe^{3+}; m = 2)$ is $\sim 2:1$. It corresponds to the Grenier phase, in which the ratio of the layers with the octahedral and tetrahedral oxygen environment is 2:1 [17,28,35]. With the increase of the Ca concentration, the contributions by the remaining subspectra tend to zero. It can be concluded that in the annealed samples, starting from $x = 0.5$, oxygen and the vacancies start being restructured for forming vacancy-ordered phases.

For comparison, Figure 6 shows dependences on the Ca concentration for the average number of the oxygen vacancies $n(\square)$ and the oxygen ions $n(O^{2-})$ (a) as well as the cations Fe^{4+} $n(Fe^{4+})$ (b) in the nearest anion and cation environments of the Fe atom for the as-prepared and vacuum-annealed orthoferrites $La_{1-x}Ca_xFeO_{3-y}$, which are calculated according to (3).

As it is clear, in the area $x = 0.5$ the as-prepared (as-pr) samples exhibit a typical specific feature that is almost unmanifested in the annealed samples. This specific feature is related to presence of the ions Fe^{4+} in the nearest cation environment of the Fe atom (Figure 6, b). In the annealed samples, in which the ions Fe^{4+} are very few, the dependence of the number of the vacancies (and of the ions O^{2-}, respectively) on the Ca concentration becomes almost linear (Figure 6, a).

Fitting of the Mössbauer spectra within the framework of the selected model for the as-prepared samples and the samples annealed in vacuum at 650 °C (650AV) has resulted in determining the hyperfine parameters H_{hf}, δ and ε for all the subspectra. Table 2 shows values of these parameters for the subspectra of the ions Fe^{3+} with the six ($H_{hf}(Fe^{3+}; 0)$, $\delta(Fe^{3+}; 0)$, $\varepsilon(Fe^{3+}; 0)$) and the four ($H_{hf}(Fe^{3+}; 2)$, $\delta(Fe^{3+}; 2)$, $\varepsilon(Fe^{3+}; 2)$) exchange bonds $Fe^{3+}{-}O^{2-}{-}Fe^{3+}$ that are typical for the extreme compositions of the studied system — $LaFeO_3$ and $CaFeO_{2.5}$ as well as for the subspectrum of the ions Fe^{4+} ($H_{hf}(Fe^{4+})$, $\delta(Fe^{4+})$, $\varepsilon(Fe^{4+})$).

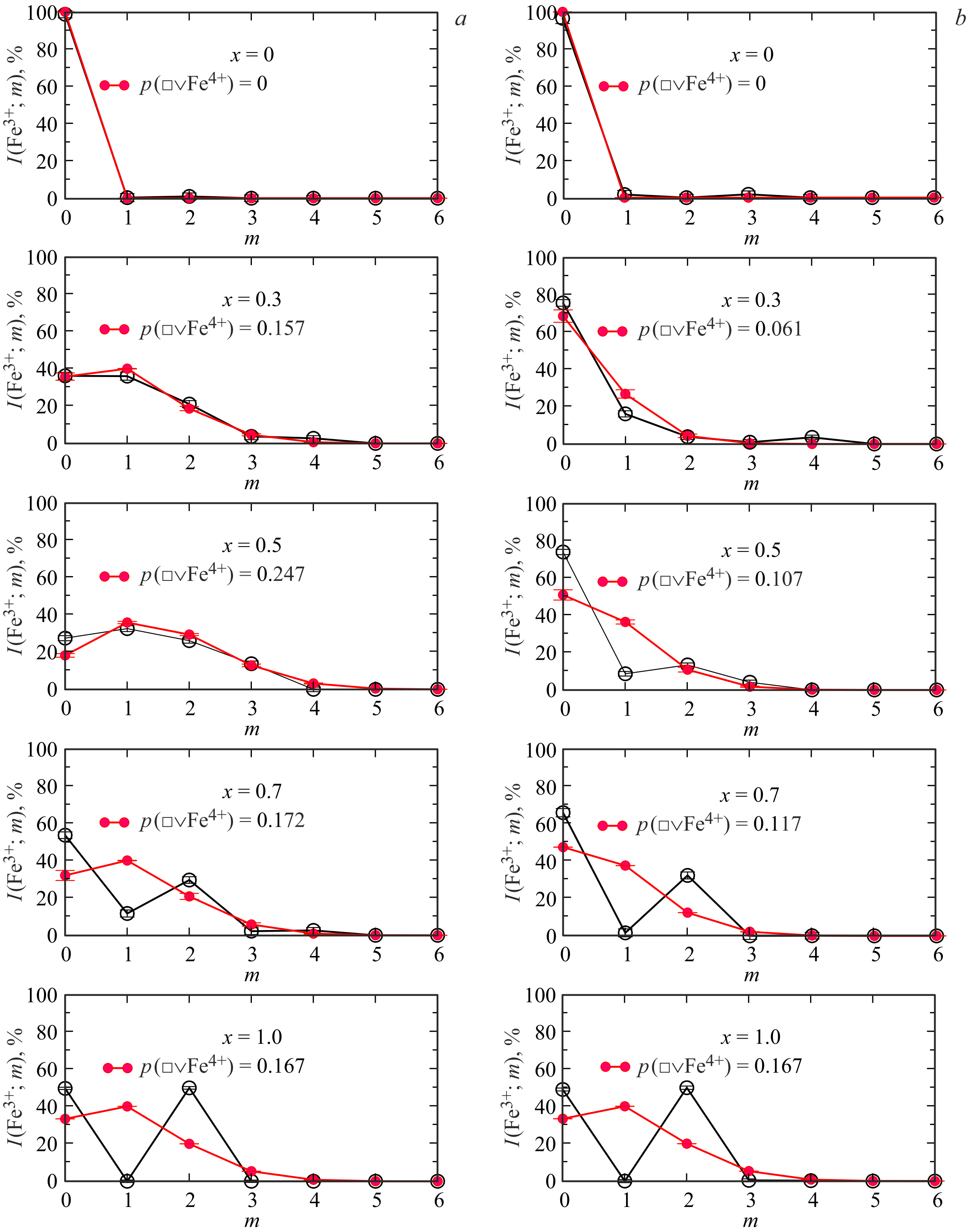

Figure 5. Dependences of relative areas $I(Fe^{3+}; m)$ (the black circles connected by lines) of the subspectra of the Fe^{3+} atoms on the number m of breaks or weakening of the exchange bonds, as induced by appearance of either the oxygen vacancies or the ions Fe^{4+} for the samples $La_{1-x}Ca_xFeO_{3-\gamma}$: *a*) the as-prepared ones and *b*) those annealed in vacuum at 650 °C. The red color marks binomial distributions of the number m of breaks or weakening of the exchange bonds.

Table 2. Values of the hyperfine (HF) parameters of the subspectra of the ions Fe^{3+} with the six ($H_{hf}(Fe^{3+}; 0)$, $\delta(Fe^{3+}; 0)$, $\varepsilon(Fe^{3+}; 0)$) and the four ($H_{hf}(Fe^{3+}; 2)$, $\delta(Fe^{3+}; 2)$, $\varepsilon(Fe^{3+}; 2)$) exchange bonds $Fe^{3+}-O^{2-}-Fe^{3+}$ as well as the subspectrum of the ions Fe^{4+} ($H_{hf}(Fe^{4+})$, $\delta(Fe^{4+})$, $\varepsilon(Fe^{4+})$—bf) for the as-prepared samples and the samples that are annealed in vacuum at 650 °C (650AV), of the orthoferrites $La_{1-x}Ca_xFeO_{3-\gamma}$

As-prepared sample					
HF-parameters	$x = 0.0$	$x = 0.3$	$x = 0.5$	$x = 0.7$	$x = 1.0$
$H_{hf}(Fe^{3+}; 0)$, kOe	556.6(6)	546.9(1.5)	544.7(1.8)	545.0(2.2)	540.1(6)
$\delta(Fe^{3+}; 0)$, mm/s	0.433(2)	0.432(7)	0.440(10)	0.477(8)	0.432(3)
$\varepsilon(Fe^{3+}; 0)$, mm/s	−0.037(2)	−0.027(7)	−0.071(9)	−0.146(8)	−0.275(2)
$H_{hf}(Fe^{3+}; 2)$, kOe	–	506.0(1.9)	491.5(2.0)	467.9(2.4)	473.2(6)
$\delta(Fe^{3+}; 2)$, mm/s	–	0.369(11)	0.411(9)	0.317(16)	0.245(3)
$\varepsilon(Fe^{3+}; 2)$, mm/s	–	0.002(11)	0.008(9)	0.326(15)	0.354(2)
$H_{hf}(Fe^{4+})$, kOe	–	256(2)	264(1)	250(4)	–
$\delta(Fe^{4+})$, mm/s	–	−0.07(2)	−0.08(2)	−0.02(6)	–
$\varepsilon(Fe^{4+})$, mm/s	–	0.00(2)	−0.01(2)	0.00(0)	–
650AV					
HF-parameters	$x = 0.0$	$x = 0.3$	$x = 0.5$	$x = 0.7$	$x = 1.0$
$H_{hf}(Fe^{3+}; 0)$, kOe	566.8(1.1)	552.3(1.0)	560.2(1.2)	554.1(2.0)	537.5(6)
$\delta(Fe^{3+}; 0)$, mm/s	0.463(3)	0.440(3)	0.448(4)	0.483(8)	0.445(3)
$\varepsilon(Fe^{3+}; 0)$, mm/s	−0.033(3)	−0.010(3)	−0.025(4)	−0.169(8)	−0.265(3)
$H_{hf}(Fe^{3+}; 2)$, kOe	–	505.4(2.5)	479.4(2.1)	475.2(2.2)	471.5(6)
$\delta(Fe^{3+}; 2)$, mm/s	–	0.318(25)	0.354(21)	0.273(17)	0.265(3)
$\varepsilon(Fe^{3+}; 2)$, mm/s	–	−0.010(3)	0.232(21)	0.328(16)	0.348(3)
$H_{hf}(Fe^{4+})$, kOe	–	253(13)	273(7)	–	–
$\delta(Fe^{4+})$, mm/s	–	−0.06(0)	−0.06(0)	–	–
$\varepsilon(Fe^{4+})$, mm/s	–	0.01(0)	0.00(0)	–	–

The values of the hyperfine parameters are followed by bracketed standard deviations of their statistical errors, which were zero in case of fixation of the parameters.

As follows from Table 2, for the hyperfine magnetic fields $H_{hf}(Fe^{3+}; 0)$, when the ions La^{3+} are substituted with the ions Ca^{2+} there is their decrease by ~ 20 kOe, which is induced by a change of the magnetic ordering temperature due to reduction of the average number of the exchange bonds $Fe^{3+}-O^{2-}-Fe^{3+}$. With the increase of the concentration of Ca^{2+}, the shifts $\delta(Fe^{3+}; 0)$ are almost unchanged, since they are first of all determined by availability of the nearest octahedral oxygen environment. At the same time, the values of $\delta(Fe^{3+}; 0)$ are close to respective values of the shift δ for the unsubstituted ferrite $LaFeO_3$, in which all the ions Fe^{3+} are involved in all the six exchange bonds $Fe^{3+}-O^{2-}-Fe^{3+}$. The most noticeable changes with the increase of the concentration of the ions Ca^{2+} are observed for the quadrupole shifts $\varepsilon(Fe^{3+}; 0)$ and induced by heterovalent substitution of La^{3+} with Ca^{2+} and, as a result, the increase of a heterogeneity degree (a gradient modulus) of the electric field within an area of arrangement of the ions Fe^{3+} and their Fe^{57} nuclei.

For the hyperfine parameters of the subspectra of the ions Fe^{3+} with the four exchange bonds $Fe^{3+}-O^{2-}-Fe^{3+}$ that originate when substituting La^{3+} with Ca^{2+}, with the increase of the Ca concentration there is a decrease of the hyperfine magnetic field $H_{hf}(Fe^{3+}; 2)$ and the shift $\delta(Fe^{3+}; 2)$ as well as an increase of the quadrupole shift $\varepsilon(Fe^{3+}; 2)$, whose values approach the values of the hyperfine parameters of the ion Fe^{3+} in the tetrahedral site of the calcium orthoferrite $CaFeO_{2.5}$ (Table 1).

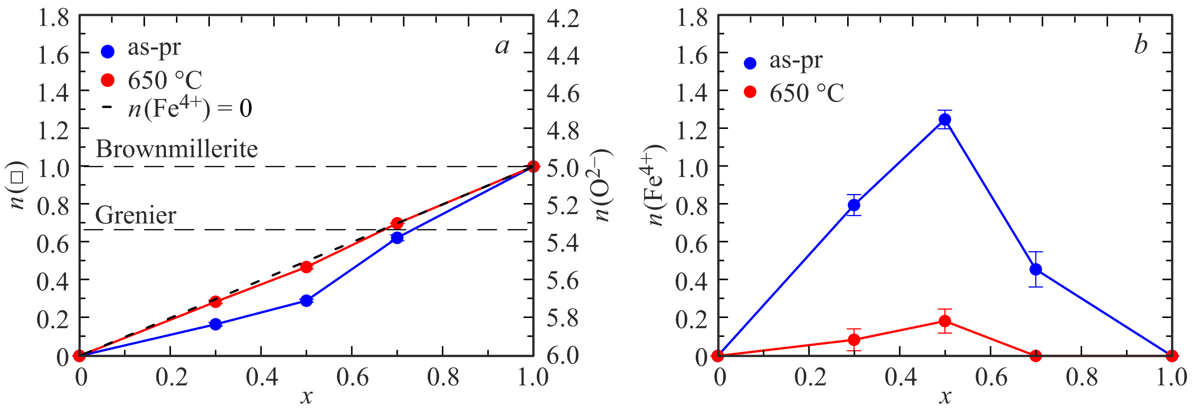

Figure 6. Dependences on the Ca concentration for the average number *a*) of the oxygen vacancies $n\square$ and the oxygen ions $n(O^{2-})$ and *b*) of the cations Fe^{4+} nFe^{4+} in the nearest anion and cation environments of the Fe atoms in the as-prepared (as-pr) and vacuum-annealed orthoferrites $La_{1-x}Ca_xFeO_{3-\gamma}$.

The Mössbauer spectra of the concentration dependences of the parameters $\Delta H_{hf}(Fe^{3+})$, $\Delta\delta(Fe^{3+})$ and $\Delta\varepsilon(Fe^{3+})$ obtained as a result of model fitting are analyzed to show that during either break or weakening of one exchange bond $Fe^{3+}-O^{2-}-Fe^{3+}$ the hyperfine field $H_{hf}(Fe^{3+})$ and the isomer shift $\delta(Fe^{3+})$ decrease — the field by 20–40 kOe, the shift by 0.03–0.1 mm/s, while the quadrupole shift $\varepsilon(Fe^{3+})$ increases by 0–0.3 mm/s. At the same time, the changes of the field, the shift and the quadrupole shift increase with the increase of the concentration of Ca^{2+} for the as-prepared samples, starting from $x = 0.5$, and they increase for the annealed samples, starting from $x = 0.3$.

The above-described behavior of the hyperfine parameters of the Mössbauer subspectra of the ions Fe^{3+} is related both to formation of the vacancy-ordered phases, which results in a significant change of the local structure of the orthoferrites, and to noticeable distortions of the crystal lattice due to the difference in the ionic radii of La and Ca.

4. Conclusion

X-ray diffraction and Mössbauer spectroscopy were used to study the specific features of the structure of the substituted lanthanum ferrite $La_{1-x}Ca_xFeO_{3-\gamma}$ both in the synthesized state as well as after vacuum annealing at 650 °C, in a dependence on the Ca content ($x = 0-1.0$). Based on the obtained results, we have analyzed the quantitative ratio of the various nearest environments of the ions Fe^{3+} in a dependence on the Ca concentration and their redistribution during vacuum annealing. The following conclusions can be made based on the analysis of the experimental data.

- With the increase of the Ca concentration, there is the decrease of the crystal lattice volume per one formula unit V_{cell}; vacuum annealing results in its increase.
- The sample with a low content of calcium $La_{0.7}Ca_{0.3}FeO_{3-\gamma}$ as well as the pure lanthanum ferrite $LaFeO_3$ has the orthorhombic structure, which is unchanged after vacuum annealing, too. The substituted ferrites with the high content calcium ($x = 0.5$ and 0.7) are two-phase ones, wherein in the as-prepared state they contain the phases *Pbnm* and Grenier, while in the annealed state they contain the phases Grenier and $Pm\overline{3}m$. The transformation $Pbnm \rightarrow Pm\overline{3}m$ in the samples when $x \geq 0.5$ seems to be related to formation of the microdomain structure that consists of the disoriented domains with sizes of several tens of nanometers and is pictured as a perovskite cube in an X-ray pattern. This fact is described in detail in the literature [28–31,36].
- The low-temperature Mössbauer data were taken to determine the amount of each valence state of Fe, the number of the oxygen vacancies and the oxygen content for all the studied samples. In the as-prepared samples, the maximum number of the ions Fe^{4+} is possessed by the sample when $x = 0.5$.
- It is shown that with the increase of the Ca concentration, the contributions into the Mössbauer spectrum by various structure states of Fe^{3+} are redistributed; besides, the distribution ratio changes during vacuum annealing. It is shown based on comparison with the model of random contribution distribution that both in the as-prepared and annealed samples of the ferrites when $x \geq 0.7$ oxygen and the vacancies are restructured to form the vacancy-ordered phases and this restructuring is also observed in the sample when $x = 0.5$ after vacuum annealing.
- Vacuum annealing results in the decrease of the number of the various local environments of the ions Fe^{3+}, i.e. makes the structure less defective.

Acknowledgments

The authors are grateful to the Center for Collective Use of Scientific Equipment of ISSP RAS for providing experimental facilities for conducting structural research.

Funding

The study is supported by the Ministry of Science and Higher Education of the Russian Federation under State assignment by Osipyan Institute of Solid State Physics RAS (075-00370-24-04).

Conflict of interest

The authors declare that they have no conflict of interest.

References

[1] M. High, C.F. Patzschke, L. Zheng, D. Zeng, O. Gavalda-Diaz, N. Ding, K.H.H. Chien, Z. Zhang, G.E. Wilson, A.V. Berenov, S.J. Skinner, K.L. Sedransk Campbell, R. Xiao, P.S. Fennell, Q. Song. Nature Commun. **13**, *1*, 5109 (2022).
[2] S. Hu, L. Zhang, H. Liu, Z. Cao, W. Yu, X. Zhu, W. Yang. J. Power Sources **443**, 227268 (2019).
[3] D. Mishra, J. Nanda, S. Parida, K.J. Sankaran, S. Ghadei. J. Sol-Gel Sci. Technol. **111**, *2*, 381 (2024). https://doi.org/10.1007/s10971-024-06452-3
[4] N. Suresh Kumar, K. Chandra Babu Naidu. J. Materiomics **7**, *5*, 940 (2021). https://doi.org/10.1016/j.jmat.2021.04.002
[5] X. Su, H. Shan, Y. Tian, W. Guo, P. Zhao, L. Xue, Y. Zhang. J. Environ. Chem. Eng. **13**, *3*, 116517 (2025)
[6] P. Goel, S. Sundriyal, V. Shrivastav, S. Mishra, D.P. Dubal, K.-H. Kim, A. Deep. Nano Energy **80**, 105552 (2021). https://doi.org/10.1016/j.nanoen.2020.105552
[7] E.K. Abdel-Khalek, D.A. Rayan, A.A. Askar, M.I.A. Abdel Maksoud, H.H. El-Bahnasawy. J. Sol-Gel Sci. Technol, **97**, *1*, 27 (2021).
[8] Y. Shin, K.-Y. Doh, S.H. Kim, J.H. Lee, H. Bae, S.-J. Song, D. Lee. J. Mater. Chem. A **8**, *9*, 4784 (2020). https://doi.org/10.1039/c9ta12734h
[9] J.B. Goodenough. In: Progress in Solid State Chemistry, v. 5 / Ed. H. Reiss. Pergamon, London (1971). P. 145.
[10] J.B. Goodenough. In: Magnetism and the Chemical Bond, v. 1 / Ed. F. Albert Cotton. Interscience, London (1963). P. 154
[11] P.D. Battle, N.C. Gibb, S. Nixon. J. Solid State Chem. **79**, *1*, 75 (1989).
[12] V.D. Sedykh, O.G. Rybchenko, A.I. Dmitriev, V.I. Kulakov, A.M. Gapochka, V.S. Rusakov. Phys. Solid State **66**, *11*, 1189 (2024).
[13] M. Romero, R.W. Gómez, V. Marquina, J.L. Pérez-Mazariego, R. Escamilla. Physica B **443**, 90 (2014).
[14] S. Palimar, S.D. Kaushik, V. Siruguri, D. Swain, A.E. Viegas, C. Narayana, N.G. Sundaram. Dalton Trans. **45**, *34*, 13547 (2016).
[15] J.E. Auckett, G.J. McIntyre, M. Avdeev, H. De Bruyn, T.T. Tan, S. Li, C.D. Ling. J. Appl. Cryst. **48**, *1*, 273 (2015).
[16] R. Ghani, M.S. Mahboub, S. Zeroual, M. Mimouni, O. Ben Ali, B. Hani, M. Ghougali. Phys. Chem. Solid State **23**, *2*, 249 (2022).
[17] J. Grenier, N. Ea, M. Pouchard, M.M. Abou-Sekkina. Mater. Res. Bull. **19**, *10*, 1301 (1984).
[18] D.J. Goossens, L.S.F. Henderson, S. Trevena, J.M. Hudspeth, M. Avdeev, J.R. Hester. J. Solid State Chem. **196**, 238 (2012). http://dx.doi.org/10.1016/j.jssc.2012.06.029
[19] V.A. Kolotygin, E.V. Tsipis, M.V. Patrakeev, J.C. Waerenborgh, V.V. Kharton. Mater. Lett. **239**, 167 (2019). https://doi.org/10.1016/j.matlet.2018.11.180
[20] V.D. Sedykh, O.G. Rybchenko, N.V. Barkovskii, A.I. Ivanov, V.I. Kulakov. FTT **63**, *10*, 1648 (2021). (in Russian). https://doi.org/10.21883/FTT.2021.10.51418.128
[V.D. Sedykh, O.G. Rybchenko, N.V. Barkovskii, A.I. Ivanov, V.I. Kulakov. Phys. Solid State **63**, *10*, 1775 (2021).]
[21] V. Sedykh, O. Rybchenko, V. Rusakov, S. Zaitsev, O. Barkalov, E. Postnova, T. Gubaidulina, D. Pchelina, V. Kulakov. J. Phys. Chem. Solids **171**, 111001 (2022). https://doi.org/10.1016/j.jpcs.2022.111001
[22] V. Sedykh, V. Rusakov, O. Rybchenko, A. Gapochka, K. Gavrilicheva, O. Barkalov, S. Zaitsev, V. Kulakov. Ceram. Int. **49**, *15*, 25640 (2023). https://doi.org/10.1016/j.ceramint.2023.05.105
[23] R.D. Shannon. Acta Cryst. A **32**, *5*, 751 (1976).
[24] M.E. Matsnev, V.S. Rusakov. AIP Conf. Proceed. **1489**, *1*, 178 (2012). https://doi.org/10.1063/1.4759488
[25] V.D. Sedykh, O.G. Rybchenko, V.S. Rusakov, A.M. Gapochka, A.I. Dmitriev, E.A. Pershina, S.V. Zaitsev, K.P. Meletov, V.I. Kulakov, A.I. Ivanov. FTT **67**, *1*, 206 (2025). (in Russian).
[26] K. Zhou, H. Cao, K. Gao, J. Shen, Z. Lu, Z. Wu, M. Liu. Modern Phys. Lett. B **37**, *35*, 2350188 (2023).
[27] A.N. Nadeev, S.V. Tsybulya, E.Yu. Gerasimov, N.A. Kulikovskaya, L.A. Isupova. J. Structural Chem. **51**, *5*, 891 (2010).
[28] P.M. Price, N.D. Browning, D.P. Butt. J. Am. Ceram. Soc. **98**, *7*, 2248 (2015). https://doi.org/10.1111/jace.13474
[29] M. Vallet-Regí, J. González-Calbet, M.A. Alario-Franco, J.-C. Grenier, P. Hagenmuller. J. Solid State Chem. **55**, *3*, 25l (1984).
[30] M.A. Alario-Franco, J.M. Gonzalez-Calbet, M. Vallet-Regí, J.-C. Grenier. J. Solid State Chem. **49**, *2*, 219 (1983).
[31] M.A. Alario-Franco, M.J.R. Henche, M. Vallet, J.M.G. Calbet, J.-C. Grenier, A. Wattiaux, P. Hagenmuller. J. Solid State Chem. **46**, *1*, 23 (1983).
[32] J.C. Grenier, L. Fournès, M. Pouchard, P. Hagenmuller, S. Komornicki. Mater. Res. Bull. **17**, *1*, 55 (1982). https://doi.org/10.1016/0025-5408(82)90183-0
[33] G.A. Sawatzky, F. van der Woude. J. Physique Colloq. **35**, *C6*, 47 (1974).
[34] V.I. Nikolaev, V.S. Rusakov. Messbauerovskie issledovaniya ferritov. Izd-vo Mosk. Un-ta, M. (1985). 224 p. (in Russian).
[35] Y. Shin, G. Galli. npj Comput. Mater. **9**, *1*, 218 (2023). https://doi.org/10.1038/s41524-023-01175-5
[36] T.C. Gibb. J. Solid State Chem. **74**, *1*, 176 (1988).

Translated by M.Shevelev